

# Dynamic Model Establishment of a Deployable Missile Control Fin with Nonlinear Hinge

Dae-Kwan Kim,<sup>\*</sup> Jae-Sung Bae,<sup>†</sup> In Lee,<sup>‡</sup> and Jae-Hung Han<sup>§</sup>

*Korea Advanced Institute of Science and Technology, Daejeon 305-701, Republic of Korea*

A deployable missile control fin has some structural nonlinearities because of the worn or loose hinges and the manufacturing tolerance. The structural nonlinearity cannot be eliminated completely, and it exerts significant effects on the static and dynamic characteristics of the control fin. Thus, it is important to establish the accurate deployable missile control fin model. In the present study, the nonlinear dynamic model of the deployable missile control fin is established. The deployable missile control fin can be subdivided into two substructures represented by linear dynamic models and a nonlinear hinge with structural nonlinearities. From dynamic tests, the nonlinear hinge parameters are identified and the nonlinear hinge model is established by the use of a system identification method such as the force-state mapping technique. The substructure modes are improved by the use of the frequency response method. The substructure models and the nonlinear hinge model are coupled to establish the nonlinear dynamic model of the fin by the use of the expanded substructure synthesis. Finally, the established nonlinear dynamic model of the deployable missile control fin is verified by modal and dynamic tests. The established model is in good agreement with test results, showing that the present approach is useful in aeroelastic stability analyses such as time-domain nonlinear flutter analysis.

## Nomenclature

$C$	=	viscous damping coefficient
$\{F\}$	=	applied force vector
$F_c$	=	coulomb damping coefficient
$K$	=	stiffness
$[K]$	=	linear stiffness matrix
$K_\theta$	=	hinge stiffness coefficient
$K_1, K_2, K_3$	=	stiffness with free play
$[k]$	=	generalized linear stiffness matrix
$M$	=	mass
$[M]$	=	linear mass matrix
$[m]$	=	generalized linear mass matrix
$P$	=	preload
$s_1, s_2$	=	free-play ( $s_2 - s_1$ ) points
$t$	=	time
$\{u\}$	=	physical displacement vector
$x$	=	displacement
$\{\xi\}$	=	generalized displacement vector
$[\Psi_C]$	=	constraint mode matrix
$[\Psi_N]$	=	normal mode matrix
$\omega$	=	natural frequency

## Subscripts

$I$	=	interface coordinate
$I_n$	=	interface coordinate without hinge stiffness
$I_p$	=	interface coordinate with hinge stiffness
$R$	=	interior coordinate

## Superscripts

$(A)$	=	substructure A
$(B)$	=	substructure B
$(\cdot)$	=	derivative with time

## I. Introduction

A DEPLOYABLE missile control fin, shown in Fig. 1, has been used primarily for the efficient use of space for the past several decades. These deployable fins are packed into each launching tube in folded state and unfolded immediately after launching. Most of deployable missile control fins have a complex hinge consisting of a torsional spring, a compression spring, and several stoppers. Because of wear and manufacturing tolerance, the hinge of the deployable control fin has some structural nonlinearities, such as preload, free play, asymmetric bilinear stiffness, hysteresis, and coulomb damping. These nonlinearities are impossible to eliminate completely, and they exert significant effects on the static and dynamic characteristics. Therefore, it is necessary to obtain the accurate dynamic model of a deployable missile control fin. However, it is difficult to apply full-order nonlinear finite element models directly to many practical engineering problems, especially when iterate analyses are required such as time-domain nonlinear flutter analysis.<sup>1,2</sup>

This paper discusses an expanded substructure synthesis method, including a nonlinear hinge model, to establish the reduced dynamic model of the deployable missile control fin with a nonlinear hinge. First, system identification is performed to establish the nonlinear mathematical model of the hinge. Second, Craig–Bampton’s component mode synthesis<sup>3</sup> is expanded to couple the constructed hinge model and the other structure models of the control fin. Finally, the effectiveness and the accuracy of the established model of the control fin are verified with modal and dynamic tests.

There have been many studies on the system identification methods to estimate parameters of the nonlinear structures from static and dynamic tests. The system identification methods can be broadly classified into the parametric methods<sup>4,5</sup> and the nonparametric methods.<sup>6–8</sup> The former identifies the parameters of the predetermined mathematical structure of the system, and the latter composes the characteristic equations of suitable functional series to represent the system.

In general, most practical engineering structures are complicated and may have some nonlinearities. Each structure can be divided

Received 10 July 2003; revision received 17 February 2004; accepted for publication 29 February 2004. Copyright © 2004 by the American Institute of Aeronautics and Astronautics, Inc. All rights reserved. Copies of this paper may be made for personal or internal use, on condition that the copier pay the \$10.00 per-copy fee to the Copyright Clearance Center, Inc., 222 Rosewood Drive, Danvers, MA 01923; include the code 0022-4650/05 \$10.00 in correspondence with the CCC.

<sup>\*</sup>Graduate Research Assistant, Department of Aerospace Engineering; dkk@asdl.kaist.ac.kr.

<sup>†</sup>Ph.D. Researcher, Department of Aerospace Engineering; bjs@asdl.kaist.ac.kr. Member AIAA.

<sup>‡</sup>Professor, Department of Aerospace Engineering; inlee@asdl.kaist.ac.kr. Senior Member AIAA.

<sup>§</sup>Assistant Professor, Department of Aerospace Engineering; jae-hung@kaist.ac.kr. Member AIAA.

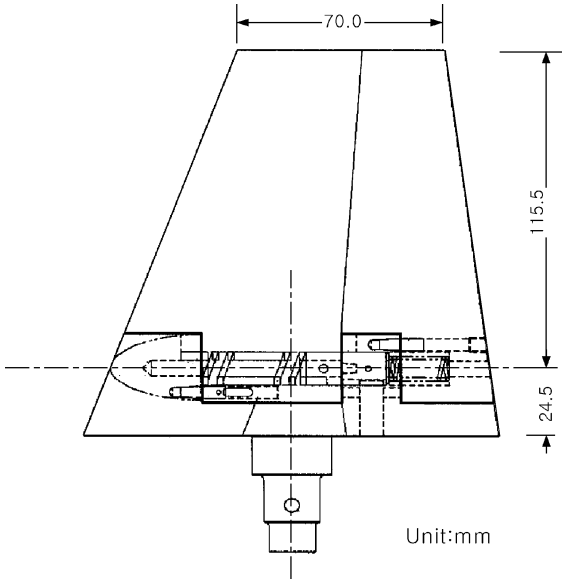


Fig. 1 Configuration of deployable missile control fin.

into linear or nonlinear substructures to simplify analysis. The information about the position of structural nonlinearity offers the opportunity to separate the structure into linear and nonlinear components, so that they can be separately analyzed for the substructure synthesis. Substructure synthesis is a modeling method that permits the representation of a relatively complex structure by a reduced number of degrees of freedom (DOF). Hunn<sup>9</sup> introduced the first partial modal coupling method. Hurty<sup>10</sup> assumed that the motion of each substructure could be expressed by a linear combination of rigid-body modes, constraint modes, and normal modes. Craig and Bampton<sup>3</sup> treated the displacements of substructures as being composed of constraint modes and normal modes. Karpel and Newman,<sup>11</sup> Karpel,<sup>12</sup> and Karpel and Raveh<sup>13</sup> suggested fictitious masses loaded at the interface coordinates of a central substructure of which the connection to the additional substructure is statically determinate. Meirovitch and Hale<sup>14</sup> introduced admissible functions to represent the motion of each substructure.

Model improvement is the process by which the preciseness of theoretical modeling is coupled with the accuracy of experimental modeling under the assumption that the measured data are correct. Model improvement methods can be broadly classified into direct methods and iterative methods. The former use the measured modal data directly to identify the parameters of the equation of motion.<sup>15,16</sup> The latter calculate iteratively the parameters by the use of the limitedly measured modal data or frequency response function (FRF) data.<sup>17–20</sup> As one of the iterative methods, Lin and Ewins<sup>21</sup> improved the theoretical model by using the limited measured FRF data and replacing the unmeasured FRF data with their analytical counterparts.

In summary, the purpose of this study is to investigate the nonlinear characteristics and establish the dynamic model of the deployable missile control fin with nonlinear hinge shown in Fig. 1. After the investigation of the existence and types of the nonlinear characteristics of the control fin from modal tests, the nonlinear hinge model of the control fin is obtained by the use of the force state mapping technique.<sup>7,8</sup> At the same time, each substructure model is improved by the use of the frequency response method.<sup>21</sup> By the use of the proposed expanded substructure synthesis method, the dynamic model of a deployable missile control fin, which consists of a nonlinear hinge and substructures, is established and verified from modal and dynamic tests.

## II. Identification of Nonlinear Hinge

The existence of nonlinear characteristics should be identified before the establishment of a dynamic model of the system. Figure 2 shows the frequency response characteristics of the deployable mis-

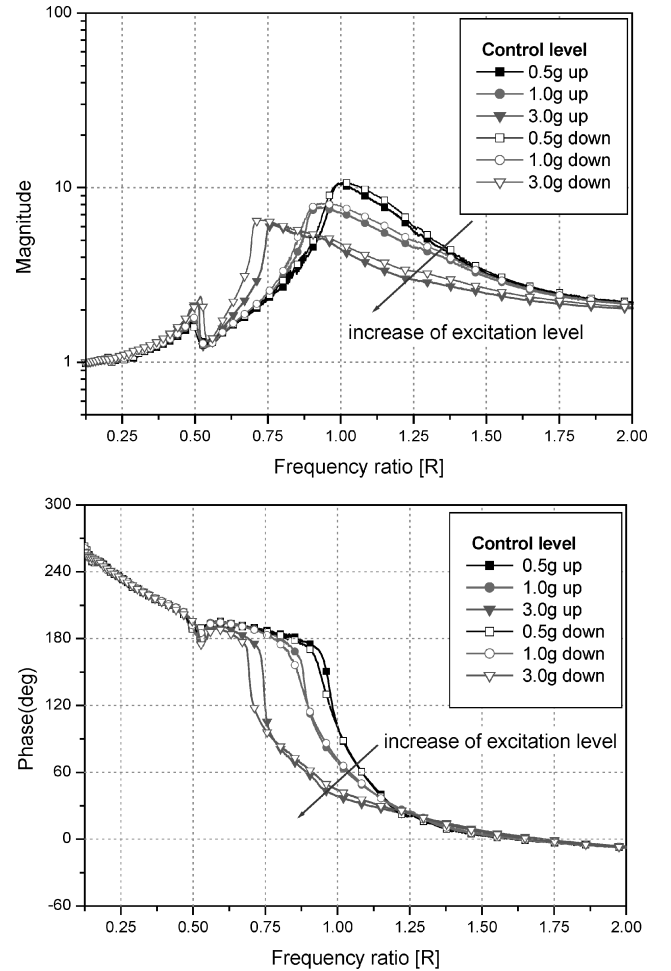


Fig. 2 Frequency responses of the control fin from the upward and downward base sine sweep.

sile control fin for a base sine-sweep excitation. The resonance frequency of the control fin is decreased as the excitation level is increased, and the variations of the response due to sweep direction can also be noticed. These observations confirm that there is a concentrated nonlinearity in the hinge. The nonlinear mathematical model of the hinge is established by the use of the following force-state mapping technique.<sup>7,8</sup>

### Force-State Mapping Technique

If the structural linkage such as a joint and hinge can be completely represented by their displacement and velocity, a single-DOF system can be expressed by the nonlinear second-order ordinary differential equation of motion as follows:

$$M\ddot{x} + C(x, \dot{x})\dot{x} + K(x, \dot{x})x = F(t) \quad (1)$$

The restoring force, which represents the force transmitted by the hinge, can be written as

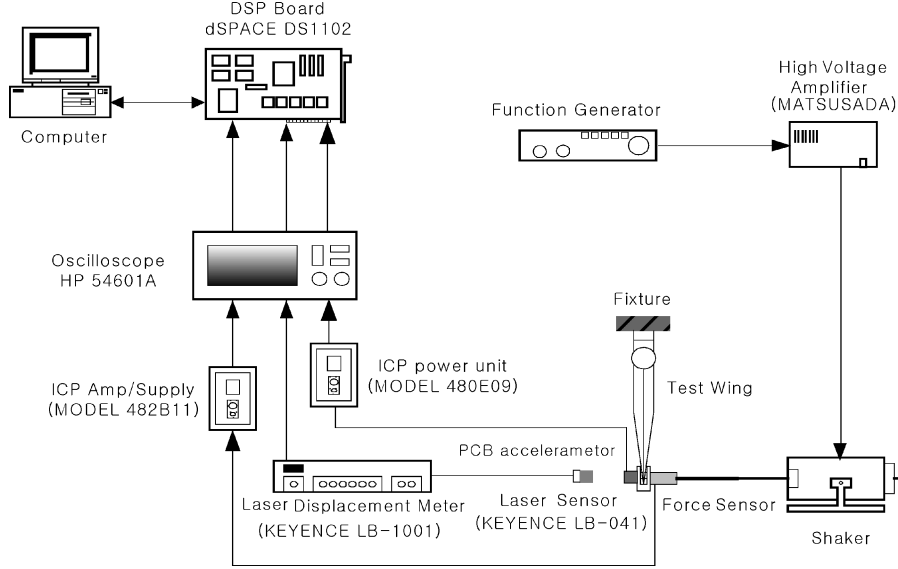
$$f(x, \dot{x}) = C(x, \dot{x})\dot{x} + K(x, \dot{x})x = F(t) - M\ddot{x} \quad (2)$$

where the restoring force  $f(x, \dot{x})$  is a function of the displacement  $x$  and velocity  $\dot{x}$ .

The force-state mapping technique is to plot the three-dimensional surface of the restoring force for the displacement and velocity. This plot is called a force-state map, and the experimental data of the displacement, velocity, acceleration, and applied force should be measured at each step to plot this map. The force-state map offers information about the linear and nonlinear dynamic properties of a hinge. If the system were linear, this map would be an inclined flat plane, but if nonlinear, it would be a curved surface. Generally,

**Table 1** Estimated parameters of the nonlinear hinge for four excitation frequencies

Frequency, Hz	$K_1$ , N · m/rad	$K_2$ , N · m/rad	$K_3$ , N · m/rad	$s_1$ , rad	$s_2$ , rad	$C_1$ , N · m · s/rad	$F_c$ , N · m	$P$ , N · m
5	365.72	65.62	436.63	-0.0050	0.0194	0.211	0.192	-0.185
15	364.42	56.17	421.84	-0.0050	0.0196	0.131	0.194	-0.105
30	366.23	60.31	410.63	-0.0047	0.0197	0.102	0.212	-0.112
50	398.33	62.78	427.26	-0.0042	0.0187	0.086	0.203	-0.030
Average	373.67	61.22	424.09	-0.0048	0.0194	0.132	0.200	-0.108

**Fig. 3** Experimental setup for dynamic test.

each of the nonlinear properties produces the different type of the force-state map, and the restoring force can be described by the linear combination of several of the linear and nonlinear force components, such as a preload, linear or nonlinear springs and dampers, coulomb friction, material hysteresis damping, and so on. Thus, an important advantage of the force-state mapping technique to be able to identify the superposable nonlinearities. However, the choice of the linear and nonlinear components depends on the experience of researcher.

### Experiments and Results

Figure 3 shows the experimental setup for the dynamic test of a missile control fin. A force sensor, a laser displacement sensor, and an accelerometer are located at the tip of the fin to measure the experimental data of the applied force, displacement, and acceleration. A shaker is used to apply the sinusoidal excitation force to the fin, and a function generator controls the frequency and amplitude of the input signal. The missile control fin is excited for four excitation frequencies and eight amplitudes for each frequency.

Figure 4 shows the force-state map of the nonlinear hinge of the fin for an excitation frequency of 30 Hz. From the curved surface of the force-state map, the nonlinearities such as preload, nonlinear stiffness with free play, and coulomb friction can be observed, and the nonlinear restoring force of the hinge can be represented by

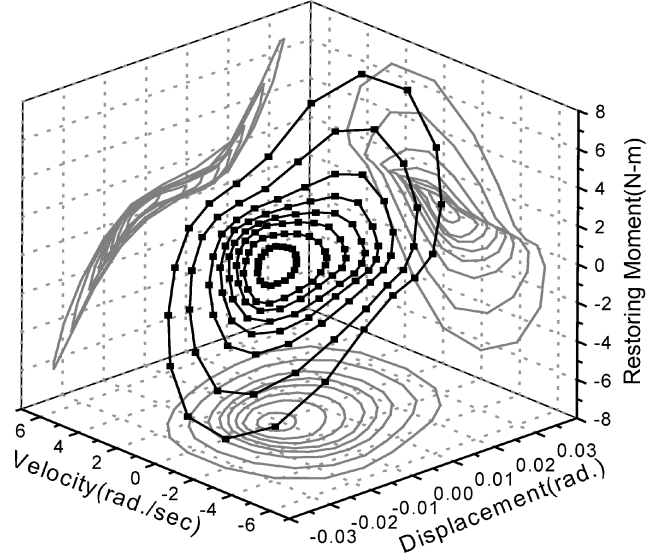
$$f = P + C_1 \dot{x} + F_c \text{sign}(\dot{x}) + F_{\text{nonlinear}} \quad (3)$$

with

$$F_{\text{nonlinear}} = \begin{cases} K_1(x - s_1), & x < s_1 \\ K_2(x - s_1), & s_1 < x < s_2 \\ K_3(x - s_2) + K_2(s_2 - s_1), & s_2 < x \end{cases}$$

The MATLAB® Optimization Toolbox is used to estimate the linear and nonlinear parameters of Eq. (3).

Table 1 shows the estimated values of the parameters of Eq. (3) for four excitation frequencies. The parameters, except for viscous

**Fig. 4** Experimentally measured force-state map of a nonlinear hinge for an excitation frequency of 30 Hz.

damping, can be assumed to have constant values over the excitation frequencies. Viscous damping decreases as the excitation frequency increases. The nonlinear hinge has the free play of 0.024 rad (1.38 deg), and the stiffness properties out of the free play are different. Figure 5 shows that the established model of the hinge is in good agreement with the dynamic test data for two excitation frequencies.

### III. Substructure Synthesis

Substructure synthesis methods have been used to reduce the number of DOF of a relatively complex structure having various configurations, so that iterative problems such as flutter can be

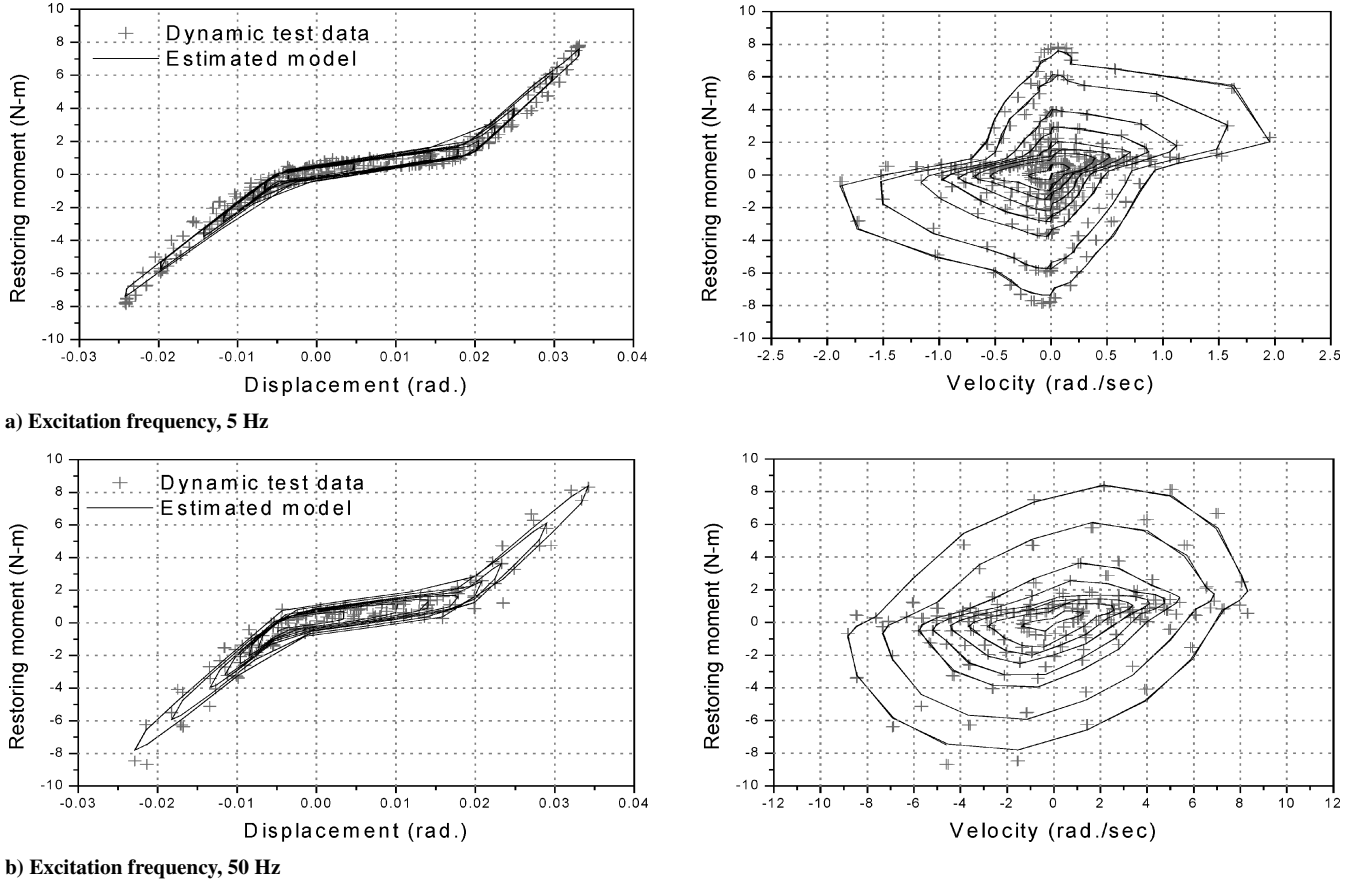


Fig. 5 Dynamic test data and estimated model of a nonlinear hinge.

efficiently analyzed with a reasonable cost and time.<sup>3,13</sup> To establish a reduced dynamic model of the missile control fin with the nonlinear hinge, we present an expanded substructure synthesis method, including nonlinear hinge models, and verified the proposed method using a plate example.

#### Substructure Synthesis Method

To analyze the dynamic characteristics of a complex structure by the use of substructure synthesis, it is necessary to divide the whole structure into a limited number of substructures. Each substructure is connected to at least one of the other substructures. For an arbitrary linear undamped substructure, the equations of motion are written as

$$\begin{bmatrix} M_{RR} & M_{RI} \\ M_{RI}^T & M_{II} \end{bmatrix} \begin{Bmatrix} \ddot{u}_R \\ \ddot{u}_I \end{Bmatrix} + \begin{bmatrix} K_{RR} & K_{RI} \\ K_{RI}^T & K_{II} \end{bmatrix} \begin{Bmatrix} u_R \\ u_I \end{Bmatrix} = \begin{Bmatrix} 0 \\ F_I \end{Bmatrix} \quad (4)$$

where the mass and stiffness matrices and displacement and force vectors are partitioned according to the interior  $R$  and interface  $I$  coordinates of the substructure. The force vector  $\{F_I\}$  is applied at the interface coordinates by adjoining substructures.

The basic assumption in the component model coupling (CB method) of Craig and Bampton<sup>3</sup> is that the displacement of each substructure can be represented by a linear combination of some normal and constraint modes. Normal modes  $[\Psi_N]$  are obtained from the eigenvalue problem with the fixed interface condition,  $\{u_I\} = 0$ , as follows:

$$[K_{RR}][\Psi_N] = [M_{RR}][\Psi_N][\omega_R^2] \quad (5)$$

where  $[\omega_R^2]$  is a diagonal matrix of the squares of natural frequencies. Constraint modes  $[\Psi_C]$  are defined as the static displacements of the interior coordinates due to successive unit displacement of interface coordinates, all other interface coordinates being totally constrained.

These modes are obtained from the static equilibrium equations as follows:

$$[K_{RR}][\Psi_C] + [K_{RI}] = [0] \quad (6)$$

The displacement vector of Eq. (4) is expressed by the use of some of the normal and constraint modes obtained from Eqs. (5) and (6), as follows:

$$\begin{Bmatrix} u_R \\ u_I \end{Bmatrix} = \begin{bmatrix} \Psi_N & \Psi_C \\ 0 & I \end{bmatrix} \begin{Bmatrix} \xi_R \\ \xi_I \end{Bmatrix} \quad (7)$$

where  $\{\xi_R \ \xi_I\}^T$  is the vector of independent generalized displacements of the substructure.

The substitution of Eq. (7) into Eq. (4), and premultiplication by the transformation matrix of Eq. (7), gives

$$\begin{bmatrix} m_{RR} & m_{RI} \\ m_{RI}^T & m_{II} \end{bmatrix} \begin{Bmatrix} \ddot{\xi}_R \\ \ddot{\xi}_I \end{Bmatrix} + \begin{bmatrix} \omega_R^2 & 0 \\ 0 & k_I \end{bmatrix} \begin{Bmatrix} \xi_R \\ \xi_I \end{Bmatrix} = \begin{Bmatrix} 0 \\ F_I \end{Bmatrix} \quad (8)$$

where

$$[m_{RR}] = [\Psi_N]^T [M_{RR}] [\Psi_N] \quad (9a)$$

$$[m_{RI}] = [\Psi_N]^T [M_{RR} \Psi_C + M_{RI}] \quad (9b)$$

$$[m_{II}] = [\Psi_C]^T \begin{bmatrix} M_{RR} & M_{RI} \\ M_{RI}^T & M_{II} \end{bmatrix} \begin{bmatrix} \Psi_C \\ I \end{bmatrix} \quad (9c)$$

$$[\omega_R^2] = [\Psi_N]^T [K_{RR}] [\Psi_N] \quad (9d)$$

$$[k_I] = [K_{II}] + [K_{RI}]^T [\Psi_C] \quad (9e)$$

The size of the matrices in Eq. (8) is the sum of the number of normal modes used and the number of interface DOF. When the

number of interface DOF is smaller than the number of rigid-body DOF of the substructure, the constraint modes  $[\Psi_C]$  are rigid-body modes that can be obtained by the application of unit displacement to each interface coordinate.

To simplify the problem, it is assumed that the whole structure consists of two substructures A and B and that substructure A adjoins the other substructure B. In the same manner, the generalized equations of motion of the substructures are written in the form A

$$\begin{bmatrix} m_{RR}^{(A)} & m_{RI}^{(A)} \\ m_{RI}^{(A)T} & m_{II}^{(A)} \end{bmatrix} \begin{Bmatrix} \ddot{\xi}_R^{(A)} \\ \ddot{\xi}_I^{(A)} \end{Bmatrix} + \begin{bmatrix} \omega_R^{2(A)} & 0 \\ 0 & k_I^{(A)} \end{bmatrix} \begin{Bmatrix} \xi_R^{(A)} \\ \xi_I^{(A)} \end{Bmatrix} = \begin{Bmatrix} 0 \\ F_I^{(A)} \end{Bmatrix} \quad (10)$$

and B

$$\begin{bmatrix} m_{II}^{(B)} & m_{RI}^{(B)T} \\ m_{RI}^{(B)} & m_{RR}^{(B)} \end{bmatrix} \begin{Bmatrix} \ddot{\xi}_I^{(B)} \\ \ddot{\xi}_R^{(B)} \end{Bmatrix} + \begin{bmatrix} k_I^{(B)} & 0 \\ 0 & \omega_R^{2(B)} \end{bmatrix} \begin{Bmatrix} \xi_I^{(B)} \\ \xi_R^{(B)} \end{Bmatrix} = \begin{Bmatrix} F_I^{(B)} \\ 0 \end{Bmatrix} \quad (11)$$

There must be at least one or more independent generalized interface coordinates to combine the substructures. Compatibility conditions are needed to ensure that the displacements and reaction forces on the interface coordinates of a substructure match those of its adjoining substructures. The compatibility equations related to the interface coordinates of the two substructures can be written as follows:

$$\{u_I^{(A)}\} = \{u_I^{(B)}\} = \{u_I\} \quad (12)$$

$$\{\xi_I^{(A)}\} = \{\xi_I^{(B)}\} = \{\xi_I\} \quad (13)$$

$$\{F_I^{(A)}\} = -\{F_I^{(B)}\} \quad (14)$$

Substitution of Eqs. (13) and (14) into Eqs. (10) and (11) and coupling these equations gives

$$\begin{bmatrix} m_{RR}^{(A)} & m_{RI}^{(A)} & 0 \\ m_{RI}^{(A)T} & m_{II}^{(A)} + m_{II}^{(B)} & m_{RI}^{(B)T} \\ 0 & m_{RI}^{(B)} & m_{RR}^{(B)} \end{bmatrix} \begin{Bmatrix} \ddot{\xi}_R^{(A)} \\ \ddot{\xi}_I \\ \ddot{\xi}_R^{(B)} \end{Bmatrix} + \begin{bmatrix} \omega_R^{2(A)} & 0 & 0 \\ 0 & k_I^{(A)} + k_I^{(B)} & 0 \\ 0 & 0 & \omega_R^{2(B)} \end{bmatrix} \begin{Bmatrix} \xi_R^{(A)} \\ \xi_I \\ \xi_R^{(B)} \end{Bmatrix} = \{0\} \quad (15)$$

The natural frequencies and eigenvectors of the combined structure can be easily obtained from Eq. (15). The transformation matrix from the generalized displacements to the physical displacements is

$$\begin{Bmatrix} u_R^{(A)} \\ u_I \\ u_R^{(B)} \end{Bmatrix} = \begin{bmatrix} \Psi_N^{(A)} & \Psi_C^{(A)} & 0 \\ 0 & I & 0 \\ 0 & \Psi_C^{(B)} & \Psi_N^{(B)} \end{bmatrix} \begin{Bmatrix} \xi_R^{(A)} \\ \xi_I \\ \xi_R^{(B)} \end{Bmatrix} \quad (16)$$

### Expansion of Substructure Synthesis Method

To establish a mathematical dynamic model of the deployable missile control fin, the technique outlined in the preceding section is expanded to consider a hinge that consists of torsional springs.

Generally, the moment applied to rotational displacements by a torsional spring can be expressed as

$$M_\theta = K_\theta(u_i - u_j) \quad (17)$$

where  $u_i$ ,  $u_j$ ,  $K_\theta$ , and  $M_\theta$  are two independent rotational displacements, namely, the torsional spring coefficient and moment, respectively. If the two substructures A and B are coupled by torsional

springs located at some of the interface coordinates, the interface coordinates of each substructure can be divided into the coordinates  $I_p$  with torsional springs and the other interface coordinates  $I_n$ . Then, the equations of motion of substructure A can be written as

$$\begin{bmatrix} M_{RR} & M_{RI_n} & M_{RI_p} \\ M_{RI_n}^T & M_{I_n I_n} & M_{I_n I_p} \\ M_{RI_p}^T & M_{I_n I_p}^T & M_{I_p I_p} \end{bmatrix} \begin{Bmatrix} \ddot{u}_R \\ \ddot{u}_{I_n} \\ \ddot{u}_{I_p} \end{Bmatrix} + \begin{bmatrix} K_{RR} & K_{RI_n} & K_{RI_p} \\ K_{RI_n}^T & K_{I_n I_n} & K_{I_n I_p} \\ K_{RI_p}^T & K_{I_n I_p}^T & K_{I_p I_p} \end{bmatrix} \begin{Bmatrix} u_R \\ u_{I_n} \\ u_{I_p} \end{Bmatrix} = \begin{Bmatrix} 0 \\ F_{I_n} \\ F_{I_p} \end{Bmatrix} \quad (18)$$

where the mass and stiffness matrices and displacement and force vectors are partitioned according to the interior coordinates  $R$  and two interface coordinates ( $I_p$ ,  $I_n$ ). The displacement vector of Eq. (18) is expressed by the use of some of the normal and constraint modes, as follows:

$$\begin{Bmatrix} u_R \\ u_{I_n} \\ u_{I_p} \end{Bmatrix} = \begin{bmatrix} \Psi_N & \Psi_{C_n} & \Psi_{C_p} \\ 0 & I & 0 \\ 0 & 0 & I \end{bmatrix} \begin{Bmatrix} \xi_R \\ \xi_{I_n} \\ \xi_{I_p} \end{Bmatrix} \quad (19)$$

The substitution of Eq. (19) into Eq. (18) and premultiplication by the transformation matrix of Eq. (19) gives

$$\begin{bmatrix} m_{RR}^{(A)} & m_{RI_n}^{(A)} & m_{RI_p}^{(A)} \\ m_{RI_n}^{(A)T} & m_{I_n I_n}^{(A)} & m_{I_n I_p}^{(A)} \\ m_{RI_p}^{(A)T} & m_{I_n I_p}^{(A)T} & m_{I_p I_p}^{(A)} \end{bmatrix} \begin{Bmatrix} \ddot{\xi}_R^{(A)} \\ \ddot{\xi}_{I_n}^{(A)} \\ \ddot{\xi}_{I_p}^{(A)} \end{Bmatrix} + \begin{bmatrix} \omega_R^{2(A)} & 0 & 0 \\ 0 & k_{I_n I_n}^{(A)} & k_{I_n I_p}^{(A)} \\ 0 & k_{I_n I_p}^{(A)T} & k_{I_p I_p}^{(A)} \end{bmatrix} \begin{Bmatrix} \xi_R^{(A)} \\ \xi_{I_n}^{(A)} \\ \xi_{I_p}^{(A)} \end{Bmatrix} = \begin{Bmatrix} 0 \\ F_{I_n}^{(A)} \\ F_{I_p}^{(A)} \end{Bmatrix} \quad (20)$$

In the same manner, the generalized equations of motion of substructure B are written in the form

$$\begin{bmatrix} m_{I_n I_n}^{(B)} & m_{I_n I_p}^{(B)T} & m_{RI_n}^{(B)T} \\ m_{I_n I_p}^{(B)} & m_{I_p I_p}^{(B)} & m_{RI_p}^{(B)T} \\ m_{RI_n}^{(B)} & m_{RI_p}^{(B)} & m_{RR}^{(B)} \end{bmatrix} \begin{Bmatrix} \ddot{\xi}_{I_n}^{(B)} \\ \ddot{\xi}_{I_p}^{(B)} \\ \ddot{\xi}_R^{(B)} \end{Bmatrix} + \begin{bmatrix} k_{I_n I_n}^{(B)} & k_{I_n I_p}^{(B)} & 0 \\ k_{I_n I_p}^{(B)T} & k_{I_p I_p}^{(B)} & 0 \\ 0 & 0 & \omega_R^{2(B)} \end{bmatrix} \begin{Bmatrix} \xi_{I_n}^{(B)} \\ \xi_{I_p}^{(B)} \\ \xi_R^{(B)} \end{Bmatrix} = \begin{Bmatrix} F_{I_n}^{(B)} \\ F_{I_p}^{(B)} \\ 0 \end{Bmatrix} \quad (21)$$

The compatibility equations relating to the interface coordinates ( $I_p$ ,  $I_n$ ) of the two substructures can be written as follows:

$$\{u_{I_n}^{(A)}\} = \{u_{I_n}^{(B)}\} = \{u_{I_n}\}, \quad \{\xi_{I_n}^{(A)}\} = \{\xi_{I_n}^{(B)}\} = \{\xi_{I_n}\} \quad (22)$$

$$\{F_{I_p}^{(A)}\} = [K_\theta](\{u_{I_p}^{(B)}\} - \{u_{I_p}^{(A)}\}) = [K_\theta](\{\xi_{I_p}^{(B)}\} - \{\xi_{I_p}^{(A)}\}) \quad (23)$$

$$\{F_{I_p}^{(B)}\} = -[K_\theta](\{u_{I_p}^{(B)}\} - \{u_{I_p}^{(A)}\}) = -[K_\theta](\{\xi_{I_p}^{(B)}\} - \{\xi_{I_p}^{(A)}\}) \quad (24)$$

where  $[K_\theta]$  is a diagonal matrix of the torsional spring coefficients according to each  $I_p$ .

Substitution of Eqs. (22), (23), and (24) into Eqs. (20) and (21) and coupling of these equations gives

$$\begin{aligned}
& \begin{bmatrix} m_{RR}^{(A)} & m_{RI_n}^{(A)} & m_{RI_p}^{(A)} & 0 & 0 \\ m_{RI_n}^{(A)T} & m_{I_n I_n}^{(A)} + m_{I_n I_n}^{(B)} & m_{I_n I_p}^{(A)} & m_{I_n I_p}^{(B)T} & m_{RI_n}^{(B)T} \\ m_{RI_p}^{(A)T} & m_{I_n I_p}^{(A)T} & m_{I_p I_p}^{(A)} & 0 & 0 \\ 0 & m_{I_n I_p}^{(B)} & 0 & m_{I_p I_p}^{(B)} & m_{RI_p}^{(B)T} \\ 0 & m_{RI_n}^{(B)} & 0 & m_{RI_p}^{(B)} & m_{RR}^{(B)} \end{bmatrix} \begin{Bmatrix} \ddot{\xi}_R^{(A)} \\ \ddot{\xi}_{I_n}^{(A)} \\ \ddot{\xi}_{I_p}^{(A)} \\ \ddot{\xi}_{I_p}^{(B)} \\ \ddot{\xi}_R^{(B)} \end{Bmatrix} \\
& + \begin{bmatrix} \omega_R^{2(A)} & 0 & 0 & 0 & 0 \\ 0 & k_{I_n I_n}^{(A)} + k_{I_n I_n}^{(B)} & k_{I_n I_p}^{(A)} & k_{I_n I_p}^{(B)} & 0 \\ 0 & k_{I_n I_p}^{(A)T} & k_{I_p I_p}^{(A)} + K_\theta & -K_\theta & 0 \\ 0 & k_{I_n I_p}^{(B)T} & -K_\theta & k_{I_p I_p}^{(B)} + K_\theta & 0 \\ 0 & 0 & 0 & 0 & \omega_R^{2(B)} \end{bmatrix} \begin{Bmatrix} \xi_R^{(A)} \\ \xi_{I_n}^{(A)} \\ \xi_{I_p}^{(A)} \\ \xi_{I_p}^{(B)} \\ \xi_R^{(B)} \end{Bmatrix} \\
& = \{0\} \quad (25)
\end{aligned}$$

The natural frequencies and eigenvectors of the combined structure with torsional springs can be easily obtained from Eq. (25). The

transformation matrix from the generalized displacements to the physical displacements is

$$\begin{Bmatrix} u_R^{(A)} \\ u_{I_n}^{(A)} \\ u_{I_p}^{(A)} \\ u_{I_p}^{(B)} \\ u_R^{(B)} \end{Bmatrix} = \begin{bmatrix} \Psi_N^{(A)} & \Psi_{C_n}^{(A)} & \Psi_{C_p}^{(A)} & 0 & 0 \\ 0 & I & 0 & 0 & 0 \\ 0 & 0 & I & 0 & 0 \\ 0 & 0 & 0 & I & 0 \\ 0 & \Psi_{C_n}^{(B)} & 0 & \Psi_{C_p}^{(B)} & \Psi_N^{(B)} \end{bmatrix} \begin{Bmatrix} \xi_R^{(A)} \\ \xi_{I_n}^{(A)} \\ \xi_{I_p}^{(A)} \\ \xi_{I_p}^{(B)} \\ \xi_R^{(B)} \end{Bmatrix} \quad (26)$$

### Numerical Example

To verify the present expanded substructure synthesis method, the free vibration of a cantilever plate is considered. The plate has two substructures coupled by a hinge section with four torsional springs, as shown in Fig. 6. Each node has three DOF, one translation and two rotation DOF. Each substructure, therefore, has 12 interface DOF. The torsional spring coefficient, elastic modulus, density and poisson ratio used for the example are  $K_\theta = 3 \text{ Nm/rad}$ , 72 GPa, 2800 kg/m<sup>3</sup>, and 0.33, respectively.

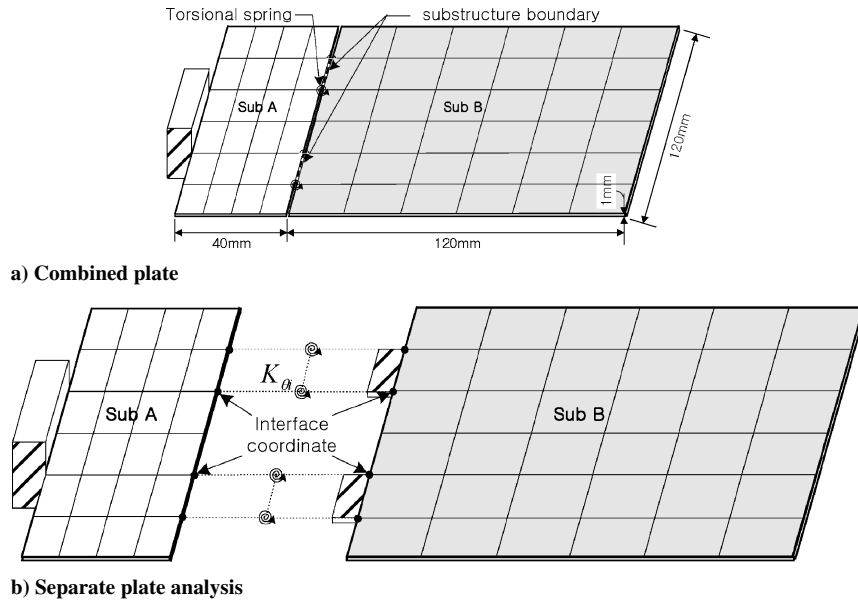
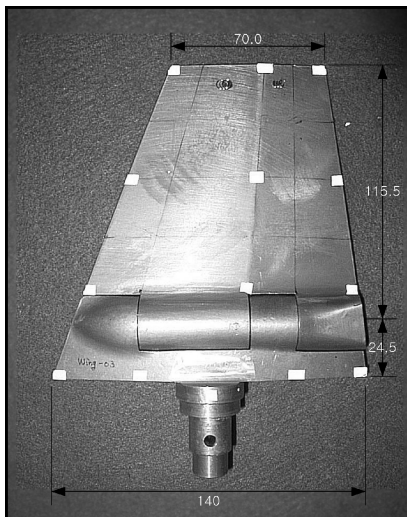
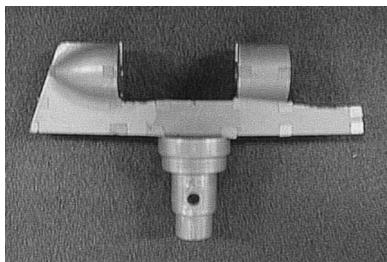


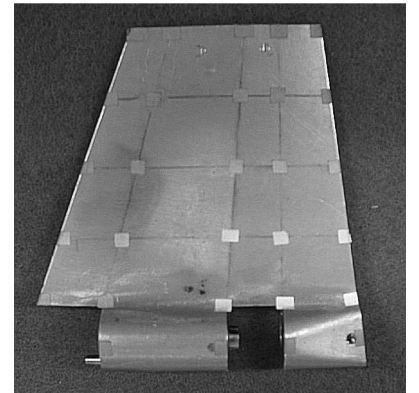
Fig. 6 Schematic of a cantilever plate with two components and four torsional springs.



a) Combined missile control fin (millimeters)



b) Substructure A (lower wing)



c) Substructure B (upper wing)

Fig. 7 Configurations of a deployable missile control fin.

The comparison is made between natural frequencies and mode shapes of the full plate calculated by the use of the MSC/NASTRAN<sup>®</sup> and corresponding natural frequencies calculated by the present expanded substructure synthesis method. The frequency range, 0–500 Hz, is selected as the frequency range of interest. The lowest three and seven modes are used to represent substructures A and B, respectively, which cover the frequency range of interest twice.

Table 2 gives the frequencies, errors, and modal assurance criteria (MAC)<sup>22</sup> obtained by the two methods indicated earlier. It is clear that the normal modes of the entire structure are accurately obtained by the use of the expanded CB method.

#### IV. Deployable Missile Control Fin

The nonlinear dynamic model of the deployable missile control fin is established and verified in this section. The finite element

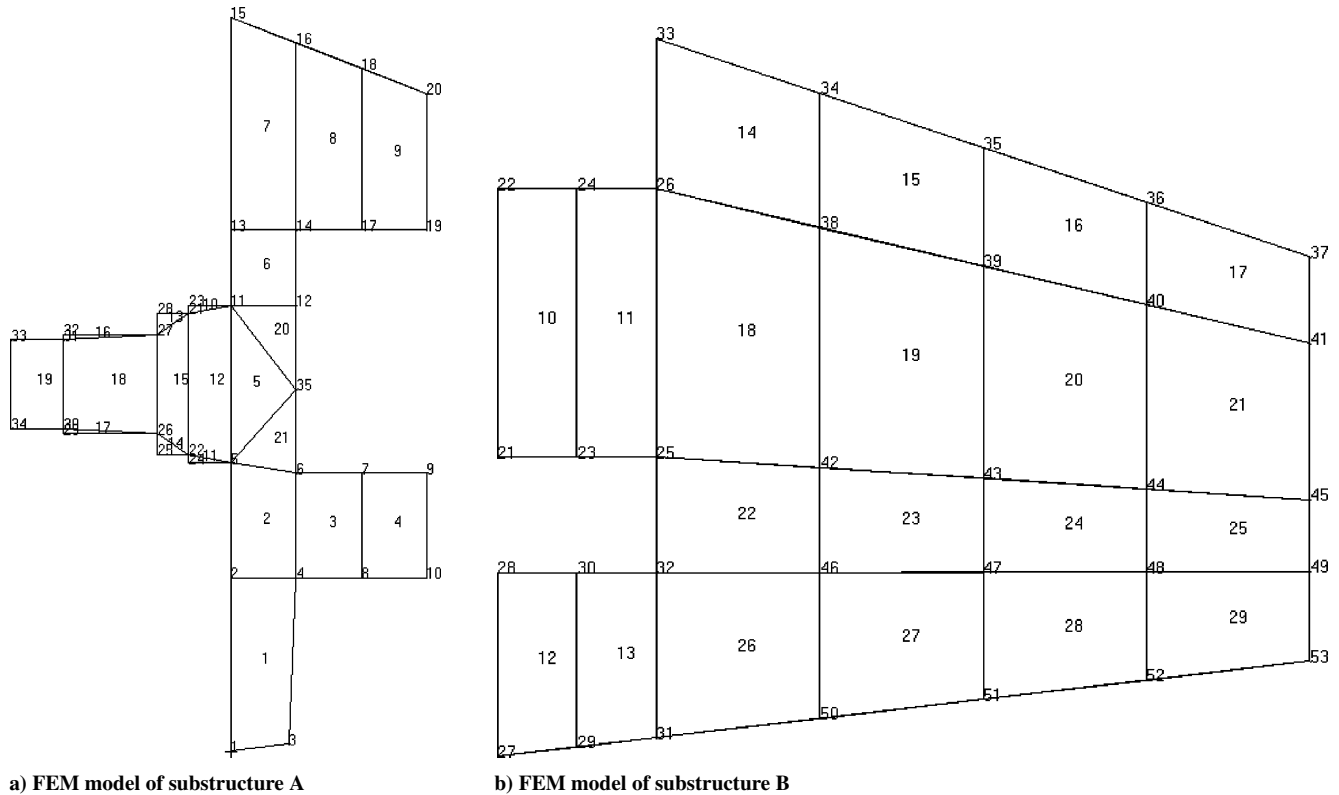


Fig. 8 Finite element method (FEM) model of substructures A and B.

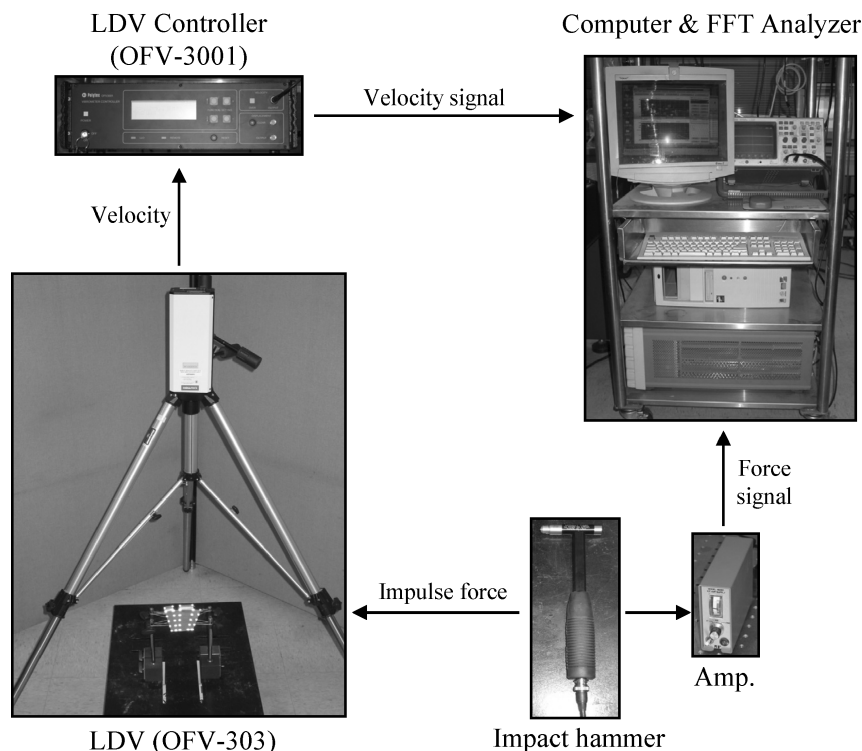
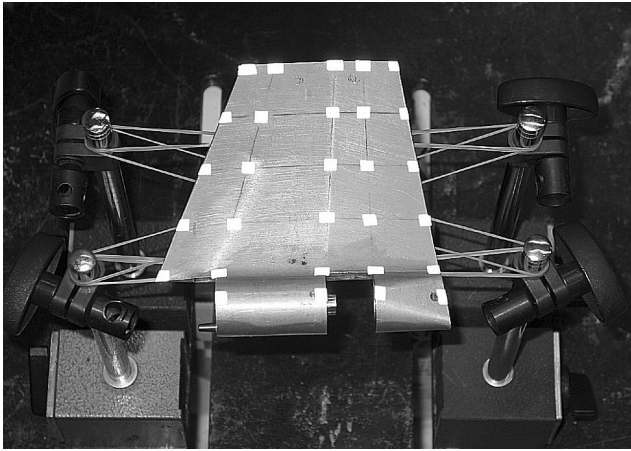
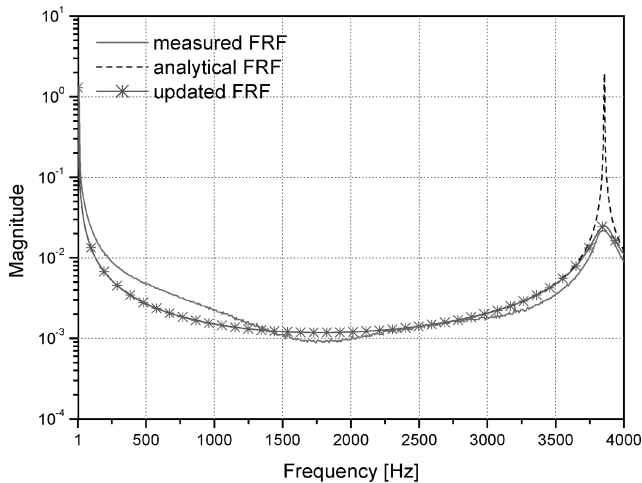
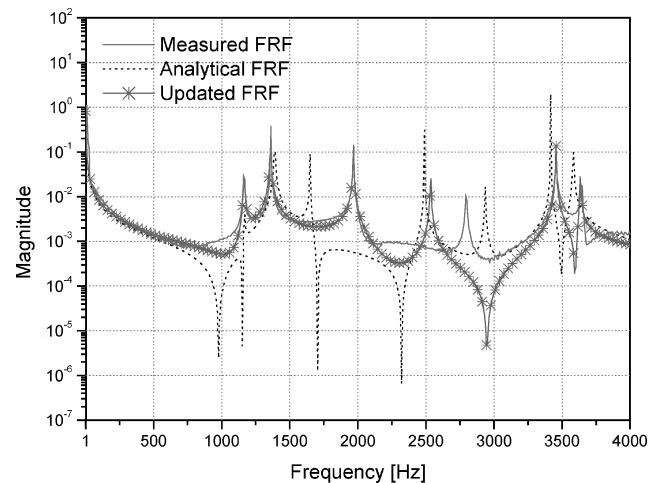
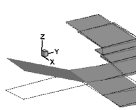
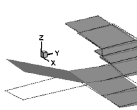



Fig. 9 Experimental setup for modal testing.

**Table 2** Comparison of natural frequency and mode shape

Mode	Full model frequency, Hz	Expanded CB frequency, Hz	Error, %	MAC
1	22.617	22.617	0.000	1.000
2	78.909	78.913	0.006	1.000
3	173.539	173.591	0.030	1.000
4	262.653	263.526	0.332	0.998
5	405.576	406.737	0.286	0.997
6	410.891	411.268	0.092	0.999
7	493.391	493.946	0.112	0.999
8	580.348	583.037	0.463	0.999
9	732.554	735.112	0.349	0.995
10	779.171	834.379	7.085	0.916

**Fig. 10** Free-boundary condition of substructures.**Fig. 11** Mobility curves of substructure A.**Fig. 13** Mobility curves of substructure B.

Mode	FEM	FRM	Exp
1st			
	3856.1Hz	3846.7Hz	3850.0Hz

**Fig. 12** First modes of substructure A.

models of upper and lower wings of the deployable missile control fin are improved by the use of the frequency response method (FRM)<sup>21</sup> from modal tests. To establish the combined model, these substructure models and the nonlinear hinge model established from the system identification process are coupled by the use of the expanded CB method. The dynamic model of the control fin is verified by modal and dynamic tests.

#### Substructure Model Improvement

The deployable missile control fin considered in this paper has a lower wing and an upper wing, which are, respectively, considered substructures A and B, as shown in Fig. 7. The finite element models of substructures A and B shown in Fig. 8 are established by the use of MSC/NASTRAN. substructure A has tria-3 and quad-4 elements and substructure B has quad-4 elements. Each node has one translation and two rotation DOF. Substructures A and B, therefore, have a total 105 and 99 DOF, respectively.

The model verifications and improvements of the substructures are performed through modal tests. Figure 9 shows the experimental setup for modal testing. Each substructure is excited with impulse forces by the use of an impact hammer. To measure the responses of the substructures without contact, a laser doppler vibrometer (LDV-Polytec OFV-3001/303), with a resolution of  $0.5 \mu\text{m/s}$  in a 10-Hz bandwidth and a maximum signal frequency of 1500 kHz, is used to measure the vertical translation velocities. The impulse force and velocity signals are analyzed by the use of a full Fourier transform (FFT) analyzer to obtain the frequency responses.

The frequency range of interest for the whole structure is selected to be from 1 Hz to 2 kHz, and the verified frequency range for each substructure is up to 4 kHz. Each test has been performed in the free-boundary condition shown in Fig. 10. The 17 vertical velocities out of 105 DOF for substructure A, and the 29 vertical velocities out of 99 DOF for substructure B are measured by the use of the LDV.

Figure 11 shows the mobility curves of the analytical, measured, and improved models of substructure A. The first mode only exists in the frequency range, and the mobility of the improved model agrees very well with that of the measured mobility. Figure 12 shows that the mode shapes of the models agree well with each other. Figure 13



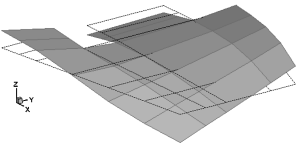
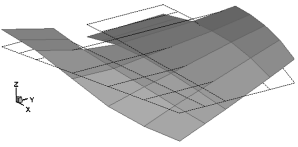
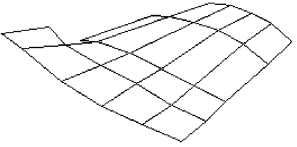
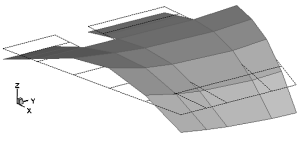
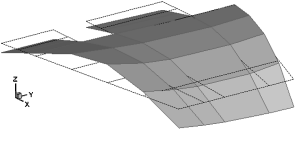
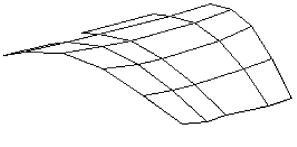
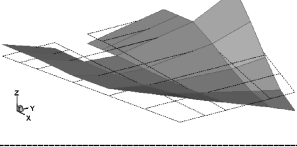
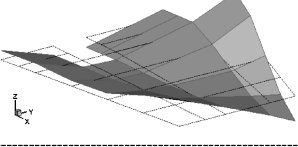
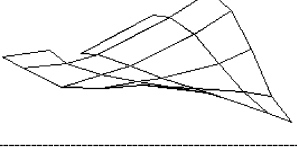
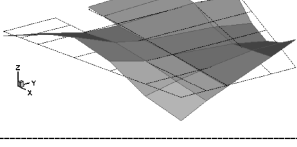
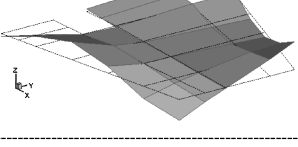
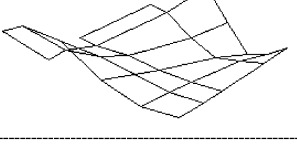
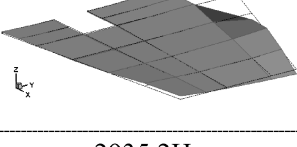
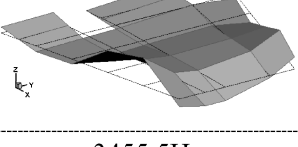

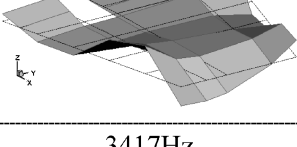
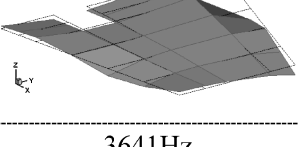
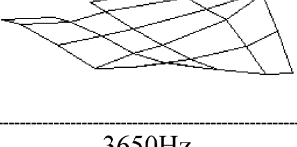
Mode	FEM	FRM	Exp.
1st			
	1165.4Hz	1164.7Hz	1160Hz
2nd			
	1389.1Hz	1358.2Hz	1360Hz
3rd			
	1650Hz	1967.5Hz	1970Hz
4th			
	2489.3Hz	2534.6Hz	2800Hz
5th			
	2935.2Hz	3455.5Hz	3460Hz
6th			
	3417Hz	3641Hz	3650Hz

Fig. 14 First six fundamental mode shapes of substructure B.

shows the mobility curves of substructure B, and the first six modes exist in the frequency range. The mobility of the improved model agrees with that of the measured mobility, except for the fourth mode. Figure 14 shows good agreement from the first to fourth modes. Note the difference between the measured and the analytical mode shapes, as well as the concordance of the measured and the refined mode shapes, at the fifth and the sixth mode.

#### Verification of Missile Control Fin Model

The improved models of substructures A and B and the nonlinear hinge model located at the interface coordinates are coupled by the use of the expanded CB method. Figure 15 shows a scheme of the coupling process. The lowest single mode of substructure A and six modes of substructure B are used to represent each substructure. The coupled structural model is verified by three verifications. In these verifications, the damping terms of the nonlinear hinge model, Eq. (3), are ignored for the application of Eq. (25).

The first verification is the comparison of natural frequencies and mode shapes calculated from Eqs. (25) and (26) for the coupled structure model with modal test results of the deployable missile control fin in the free-boundary condition. This modal test has been performed in the frequency range from 1 Hz to 4 kHz, and the vertical velocities are measured by the use of the LDV. Table 3 shows the natural frequencies of the coupled structural model calculated with three estimated linear hinge stiffness properties partitioned with the free play and corresponding measured natural frequencies. The first mode cannot be measured and has the largest variation with the hinge stiffness properties. It shows reasonable agreement from the second to the sixth mode. Figure 16 compares the mode shapes of the measured and the coupled structure model, showing good agreement of the coupled structure model with the measured.

The second verification is the comparison of the first natural frequency of the coupled structure model with the modal test results

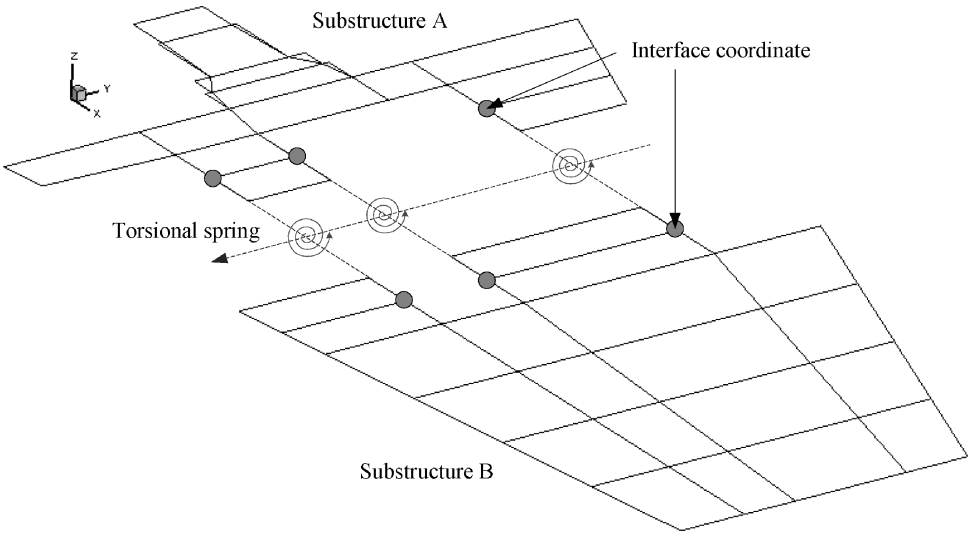


Fig. 15 Schematic diagram of substructures A, B, and nonlinear hinge model.

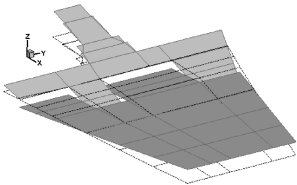
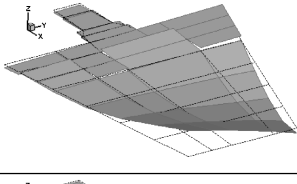

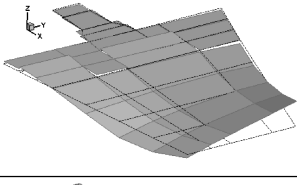
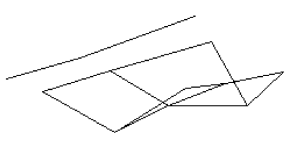
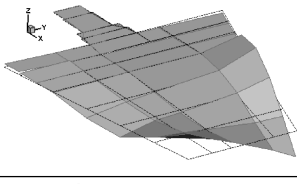
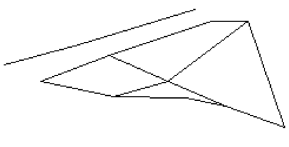
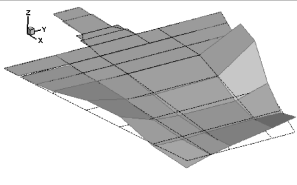
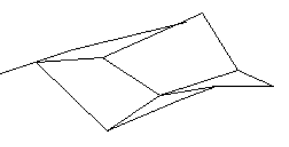
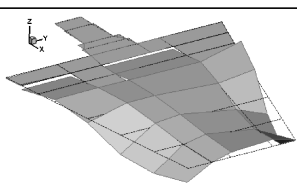
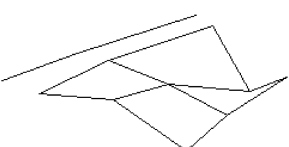
Mode	Coupled structure model	Experiment
1st		
2nd		
3rd		
4th		
5th		
6th		

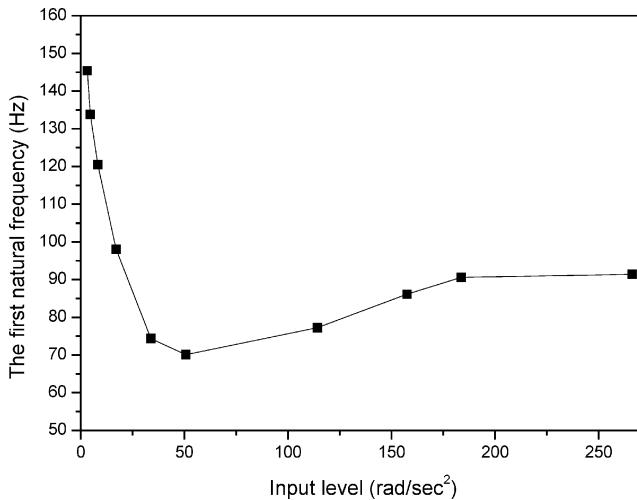
Fig. 16 First six fundamental mode shapes of the free missile control fin.

**Table 3 Comparison of synthesis and experiment natural frequencies in free-boundary condition**

Mode	Synthesis frequency, Hz			Experimental frequency, Hz
	$K_1$	$K_2$	$K_3$	
1	329.5	106.2	300.7	—
2	1283.0	1255.7	1279.5	1265
3	1457.3	1435.1	1453.8	1545
4	2788.3	2785.6	2787.9	2625
5	3415.7	3414.2	3415.5	3273
6	3735.5	3721.9	3733.7	3753

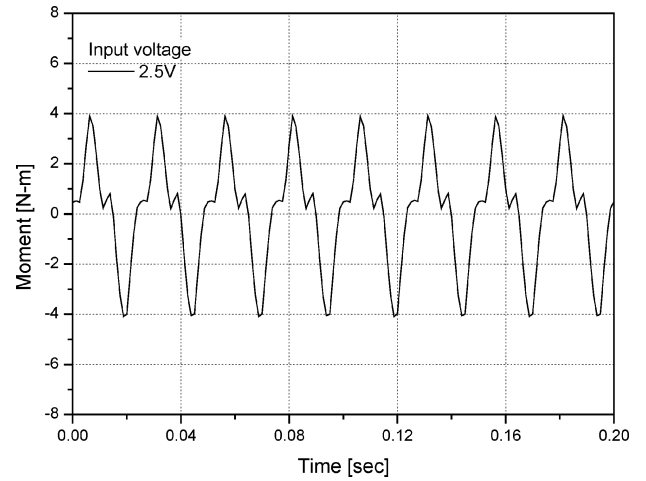
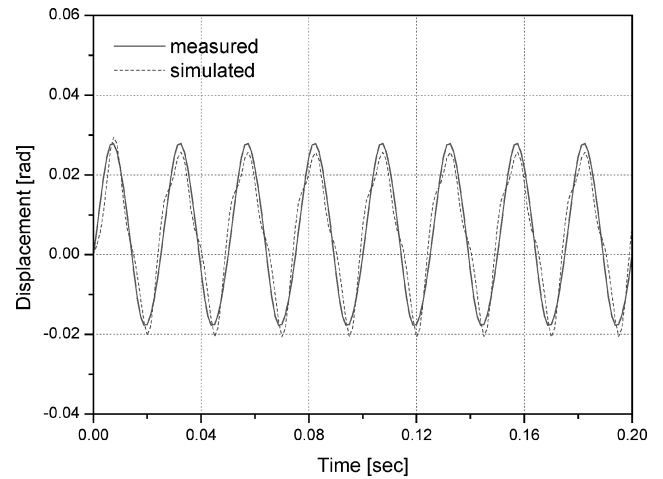
**Table 4 First natural frequency of the coupled structure model in fixed-boundary condition**

Synthesis		Experiment	
Hinge stiffness	Frequency, Hz	Input level, rad/s <sup>2</sup>	Frequency, Hz
$K_1$	154.8	3.1	145
$K_2$	61.4	50.7	70.1
$K_3$	146.4	266	91.4

**Fig. 17 First natural frequency variation of the missile control fin with fixed-boundary condition.**

for the control fin in the fixed-boundary condition. In this modal test, the lower wing of the control fin is clamped at a fixture, and a series of random excitations within the frequency range from 10 to 400 Hz is applied at the tip of the upper wing. The accelerations of the tip are measured with an accelerometer, of which transverse sensitivity is 4% and resonant frequency is 42 kHz. Table 4 shows the first natural frequencies of the coupled structural model with three stiffness properties and corresponding measured natural frequencies for several input levels. The measured natural frequencies are varied with the input levels as shown in Fig. 17, and the variation is caused by the asymmetrical bilinear hinge stiffness. It is clear that the variation of measured frequencies is within the frequency range predicted by the use of the coupled structural model.

The last verification is the comparison of the calculated time response with the dynamic test data. Figure 18 shows the input signal measured in the dynamic test, 40-Hz tip sine excitation, and the time responses of the measured and the coupled structural model for the same input signal. It shows a very good agreement between the measured and the simulated time response.

**a) Input****b) Response****Fig. 18 Input and responses of the fixed missile control fin for tip sine excitation (40 Hz).**

## V. Summary

The reduced dynamic model of the deployable missile control fin with a nonlinear hinge has been established as follows: 1) The existence of nonlinearity at the hinge of the missile control fin is investigated by executing modal tests. The parameters of the nonlinear hinge are estimated, and the mathematical nonlinear hinge model is constructed by the use of dynamic test results and the force state mapping technique. 2) To consider the hinge stiffness at the interface coordinates between the substructures, the CB component mode synthesis method is expanded. For the verification, the expanded method is applied to the clamped plate, which has redundant constraints and hinge stiffness at the interface coordinates. 3) The substructure models are improved for the natural frequencies and mode shapes with the modal test data and the frequency response method. 4) The improved finite element models of the substructures and the established nonlinear hinge model are coupled by the use of the expanded substructure synthesis method. The resulting dynamic model of the deployable missile control fin is verified with the modal test results and shows the good agreements. The coupled structural model of the deployable missile control fin is efficiently applicable to the aeroelastic analyses.

## Acknowledgments

This research was supported by the Agency for Defense Development and was partially supported by the Ministry of Science and Technology (National Research Laboratory Program) in Korea. This support is gratefully acknowledged.

## References

- <sup>1</sup>Lee, I., and Kim, S. H., "Aeroelastic Analysis of a Flexible Control Surface with Structural Nonlinearity," *Journal of Aircraft*, Vol. 32, No. 4, 1995, pp. 868–874.
- <sup>2</sup>Bae, J. S., Kim, D. K., Shin, W. H., Lee, I., and Kim, S. H., "Nonlinear Aeroelastic Analysis of a Deployable Missile Control Fin," *Journal of Spacecraft and Rockets*, Vol. 41, No. 2, 2004, pp. 264–271.
- <sup>3</sup>Craig, R., and Bampton, M., "Coupling of Structures for Dynamic Analyses," *AIAA Journal*, Vol. 6, No. 7, 1968, pp. 1313–1319.
- <sup>4</sup>Tomlinson, G. R., "Detection, Identification and Quantification of Nonlinearity in Modal Analysis-A Review," *Proceedings of 4th International Modal Analysis Conference*, 1986, pp. 837–843.
- <sup>5</sup>Masri, S. F., and Caughey, T. K., "A Nonparametric Identification Technique for Nonlinear Dynamic Problems," *Journal of Applied Mechanics*, Vol. 46, June 1979, pp. 433–447.
- <sup>6</sup>Leontaritis, I. J., and Billings, S. A., "Input-Output Parametric Models for Nonlinear Systems Part I: Deterministic Nonlinear Systems," *International Journal of Control*, Vol. 41, No. 2, 1985, pp. 303–328.
- <sup>7</sup>Crawley, E. F., and Aubert, A. C., "Identification of Nonlinear Structural Elements by Force-State Mapping," *AIAA Journal*, Vol. 24, No. 1, 1986, pp. 155–162.
- <sup>8</sup>Crawley, E. F., and O'Donnell, K. J., "Force-State Mapping Identification of Nonlinear Joints," *AIAA Journal*, Vol. 25, No. 7, 1987, pp. 100–1010.
- <sup>9</sup>Hunn, B. A., "A Method of Calculating the Normal Modes of an Aircraft," *Quarterly Journal of Mechanics*, Vol. 8, March 1955, pp. 38–58.
- <sup>10</sup>Hurty, W. C., "Dynamic Analysis of Structural Systems Using Component Modes," *AIAA Journal*, Vol. 3, No. 4, 1965, pp. 678–685.
- <sup>11</sup>Karpel, M., and Newman, M., "Accelerated Convergence for Vibration Modes Using the Substructure Coupling Method and Fictitious Coupling Masses," *Israel Journal of Technology*, Vol. 13, May 1975, pp. 55–62.
- <sup>12</sup>Karpel, M., "Efficient Vibration Mode Analysis of Aircraft with Multiple External Store Configurations," *Journal of Aircraft*, Vol. 25, No. 8, 1988, pp. 747–751.
- <sup>13</sup>Karpel, M., and Raveh, D. M., "Fictitious Mass Element in Structure Dynamics," *AIAA Journal*, Vol. 34, No. 3, 1996, pp. 607–613.
- <sup>14</sup>Meirovitch, L., and Hale, A. L., "On the Substructure Synthesis Method," *AIAA Journal*, Vol. 19, No. 7, 1981, pp. 940–947.
- <sup>15</sup>Berman, A., and Flannelly, W., "Theory of Incomplete Models of Dynamic Structures," *AIAA Journal*, Vol. 9, No. 8, 1971, pp. 1481–1487.
- <sup>16</sup>Luk, Y. W., "Identification of Physical Mass, Stiffness and Damping Matrices Using Pseudo-Inverse," *Proceedings of 5th International Modal Analysis Conference*, 1987, pp. 679–685.
- <sup>17</sup>Baruch, M., "Optimization Procedure to Correct Stiffness and Flexibility Matrices Using Vibration Tests," *AIAA Journal*, Vol. 16, No. 11, 1978, pp. 1208–1210.
- <sup>18</sup>Collins, J. D., Hart, G. C., Hasselman, T. K., and Kennedy, B., "Statistical Identification of Structures," *AIAA Journal*, Vol. 12, No. 2, 1974, pp. 185–190.
- <sup>19</sup>Chen, J. C., and Garba, J. A., "Analytical Model Improvement Using Modal Test Results," *AIAA Journal*, Vol. 18, No. 6, 1980, pp. 684–690.
- <sup>20</sup>Shin, Y. S., and Lee, I., "Investigation on Equivalent System Modeling and Dynamic Characteristics Using Reduced Models," *AIAA Journal*, Vol. 38, No. 1, 2000, pp. 102–109.
- <sup>21</sup>Lin, R. M., and Ewins, D. J., "Analytical Model Improvement Using Frequency Response Functions," *Mechanical Systems and Signal Processing*, Vol. 8, No. 4, 1994, pp. 437–458.
- <sup>22</sup>Allemang, R. J., and Brown, D. L., "A Correlation Coefficient for Modal Vector Analysis," *Proceedings of 1st International Modal Analysis Conference*, 1982, pp. 110–116.

M. Miller  
Associate Editor